2022 IEEE International Conference on Cyborg and Bionic Systems
March 24-26, 2023, Wuhan, China

QuWheeleg: Quadruped Wheeled-leg Robot Based on Electromagnetic Clutch Pulse Control

Yiming He, *Student Member, IEEE*, Chao Sun, Xiaolong Quan, Yanzhou Jin, Ruochao Wang, and Qing Shi, *Senior Member, IEEE*

2022 IEEE International Conference on Cyborg and Bionic Systems (CBS) | 978-1-6654-9028-3/23/$31.00 ©2023 IEEE | DOI: 10.1109/CBS55922.2023.10115391

***Abstract*—This paper presents a quadruped wheeled-leg mobile robot. On the basis of the planar four-bar mechanism, an active deformable wheel mechanism is designed, then optimize the deformation ratio based on genetic algorithm. We use an electromagnetic clutch for motion mode switching, which ensures the stability and reliability of robot mode switching without adding extra drive. Furthermore, we propose the electromagnetic clutch high-frequency pulse control method to ensure the continuity of the leg-form motion state. The results obtained through a series of simulations and experimental tests reveal that QuWheeleg has effective barrier crossing performance (150% BL) and high load capacity (2kg), which combines the advantages of wheel and leg motion.**

I. Introduction

As an important branch of robotics, mobile robots have broad application prospects in the exploration of unknown complex environments, such as earthquakes, nuclear radiation, fire, etc. At present, all-terrain mobile wheeled robots mainly have three structures: pure wheeled, shaped wheeled and wheeled-leg robots [1]. The pure wheeled robots can neither adapt to complex terrain nor have a better barrier-crossing capability. Due to the inequality of their wheel rim shape, the shaped wheeled robots are limited in their mobility and load capacity during the movement [2]. The wheeled-leg robot has good mobility and obstacle-crossing ability, which has been rapidly developed. It has been widely used in production and life and has also become the most popular main structure of planetary exploration vehicles nowadays.

At present, most deformation structures use additional motors to directly drive the switching process, as well as maintain wheel and leg states [3]. This method not only increases the overall energy consumption of the robot but also presents the challenge of the accuracy of deformation structures. What's more, it increases the processing cost of the robot [4]. Now, there are also other deformable wheel design methods based on origami structure [5-7]. Although they are simple in mechanism, their high requirements for wheel material leading to no potential for universal application [8]. For other deformable wheeled robots, some have powerful functions but are complex mechanisms [9], and cannot be miniaturized; some rely on terrain for wheel and leg transformation, which is not very reliable[10]. In addition, existing wheeled-leg robots are commonly driven by two-wheel differential drive with an additional tail bar at the rear [5-10], which leads to an unstable center of gravity and poor environmental adaptability due to the uncontrolled up-and-down motion of the tail bar [11,12]. Herein, we synthesize their advantages, and expect to design a small, simple, fully functional, and universally applicable active deformation mechanism to build a mobile robot platform.

In this paper, we proposed a quadruped wheeled-leg transformable robot based on electromagnetic clutch pulse control—QuWheeleg. Compared with the scheme of adding additional power, we use the electromagnetic clutch to control the deformation. Our method consumes less energy and maintains a reasonable configuration of degrees of freedom [13]. Compared with the deformation scheme based on origami structure [8], we do not need a special preparation process and material. We have reduced costs by more than five times while maintaining strength. Compared with the traditional electromagnetic clutch control method [19,20], we utilize the pulse control method to maintain the stability of the leg state without the need for precise calculation [14-16]. Finally, we take a four-bar mechanism as an example to verify the reliability of pulse-based control, which has strong robustness under complex land terrain and has the potential for universal application.

II. Robot Design

A. Design Overview

We propose a transformable structure consisting of three identical and centrally symmetric four-bar mechanisms as shown in Fig. 1. The wheel state uses the dead point position to stabilize and maintain the wheel motion form.

TABLE I. NOMENCLATURE

Variable	Definition
R_1, R_2	The radius of transformable wheel in foot and wheel
k	Deformation ratio (=R_1/R_2)
$l_1 \sim l_6$	The length of each rod in the transformable wheel
e	Eccentricity of the leg segment
x_p, z_p	Displacement of wheel center P in x, z direction
v_x, v_z	Velocity of the wheel center P in the x, z direction
s	The displacement of the wheel center P in the x direction in one cycle
F_x, F_z	The horizontal and vertical components of the fuselage's force on the front wheel
P, τ	Rated power and torque of the planetary gear motor
M	Equivalent moment of the fuselage to the front wheel

This work was supported by the National Natural Science Foundation of China under Grant 62022014.

The authors are with the Key Laboratory of Biomimetic Robots and Systems Beijing Institute of Technology, Ministry of Education, Beijing 100081, China, and also with the Intelligent Robotics Institute, School of mechatronical Engineering, Beijing Institute of Technology, Beijing 100081, China (e-mail: hym@bit.edu.cn; 1377166156@qq.com; 1958480756@qq.com; me_wangruochao@163.com; shiqing@bit.edu.cn).

978-1-6654-9028-3/23/$31.00 ©2023 IEEE

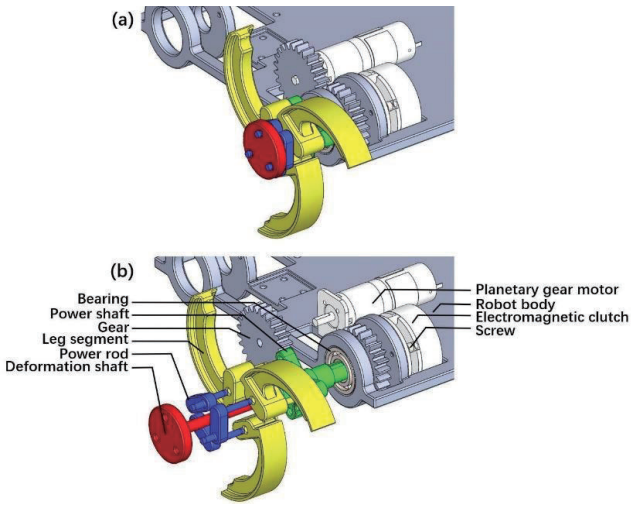

Fig. 1. Three-Dimensional explosion diagram of wheeled-leg shape reconfigurable unit.

The transformation process between the wheel state and the leg state is as follows: when the electromagnetic clutch is energized, the armature is adsorbed on the rotor and rotates with the rotor. The rotation of the deformation shaft is not restricted by the friction between the wheel and the ground, so there is no relative motion between the two axes, the wheeled-leg will not be unfolded, the robot travels in the wheel state. On the contrary, when the electromagnetic clutch is disconnected, the armature is separated from the rotor and the deformation shaft is fixed. At this time, the motor drives the power shaft through the gear drive, the relative motion is generated between the deformation shaft and the power shaft, to realize the switching between the wheel type and leg type.

B. Deformation Ratio Optimization Design

In the process of wheeled motion, to ensure the stability of the motion, we optimized the deformation ratio by using the dead point of the four-bar mechanism, limiting the length of each bar of the four-bar mechanism. The literature points out that the deformation ratio is an important design parameter for a deformable mechanism [17], which not only reflects the magnitude of deformation capacity but also indirectly reflects the overrunning capacity.

We use the deformation ratio as the objective function for single-objective optimization. The constraints are no deformation of the triangular truss, the existence of the four-bar mechanism, and the dead point limit condition mentioned above.

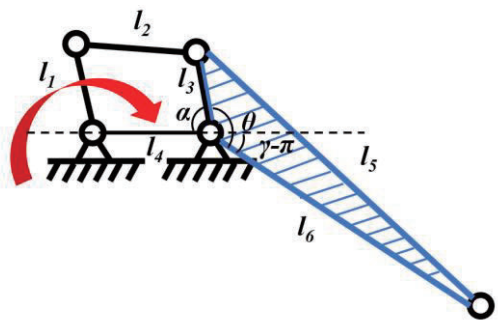

Fig. 2. Wheeled-leg shape conversion device cartesian coordinate system.

$$
\begin{cases}
\boldsymbol{max} \quad k \\
k = \dfrac{R_1}{R_2} \\
R_1 = \sqrt{\begin{matrix}[l_6\cos(\gamma-\pi)+l_4]^2 \\ +[l_6\sin(\gamma-\pi)]^2\end{matrix}} \\
{l_5}^2 = {l_3}^2 + {l_6}^2 - 2\cdot l_3\cdot l_6\cdot\cos\theta \\
{l_5}^2 = (l_3+l_4)^2 + {R_2}^2 \\
-2\cdot R_2\cdot(l_3+l_4)\cdot\cos\dfrac{2\pi}{3} \\
\sin\alpha = \dfrac{15mm}{l_4} \\
\gamma = \theta + \alpha \\
l_3 + l_6 > l_5 \\
l_3 + l_5 > l_6 \\
l_1 + l_2 = l_3 + l_4 \\
\min\limits_{1\le i\le 4} l_i + \max\limits_{1\le i\le 4} l_i \le \sum_{i_{rest}} l_i
\end{cases}
\boldsymbol{s.t.} \tag{1}
$$

We set the crossover rate as 0.75 and the mutation rate as 0.01 in the genetic algorithm. After 422 iterations, the deformation ratio increased from the initial 1.31 to 1.72, which means that the robot's ability to overcome obstacles was greatly improved.

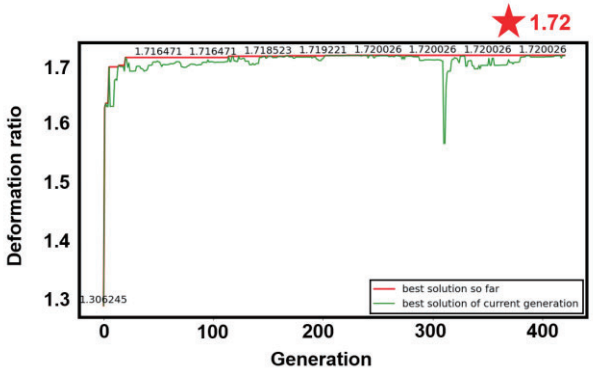

Fig. 3. Optimization results based on genetic algorithm.

In addition, we added a buckle design at the leg end, to ensure the stability of wheel motion, so that the adjacent leg bars can be closely matched.

C. Kinematic Analysis

According to the scale parameters optimized by the deformed structure in the previous section, the kinematic analysis of the deformed wheeled-leg mobile robot is carried out in this section. The displacement and velocity models of the robot's leg form forward are constructed to obtain the motion characteristics of the robot traveling in the leg form [18].

1) Traveling process on the smooth road in the leg form

Assuming that there is no slip in the y-axis direction when the mobile robot moves in the positive direction along the x-axis in leg form, each parameter of the whole moving process can be represented in the x-z plane. One of the wheels is selected for the study below.

As shown in Fig. 4, the design parameters: R=50.00mm, r=15.00mm, l=22.00mm, and b=28.00mm. It's easy to obtain:

$$\theta_1 = arctan\frac{r}{\sqrt{l^2 - r^2} + R - b} = 0.1194\pi \quad (2)$$

$$e = \sqrt{r^2 + \left(\sqrt{l^2 - r^2} + R - b\right)^2} = 40.94mm \quad (3)$$

The radius of the wheel spread is obtained from the cosine theorem.

$$R' = \sqrt{R^2 + e^2 - 2Recos\left(\theta_1 + \frac{2\pi}{3}\right)} = 85.90mm \quad (4)$$

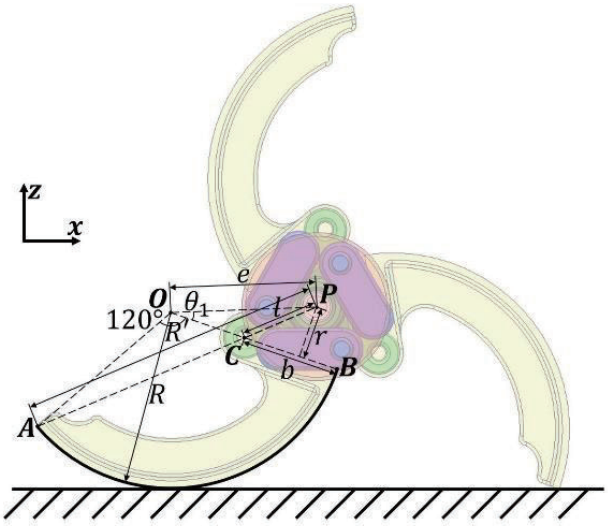

Fig. 4. Free body diagram of the wheel in leg configurations.

As the wheel turns through a week, the wheeled-leg makes three sets of repetitive motions, each of which (hereafter referred to as one cycle) turns through an angle of 2π/3. One cycle can be further divided into two phases: Phase I is the roll along the edge of the wheel $\widehat{AB}$, i.e., from state I to state II. Phase II is the rotation around endpoint A, i.e., from state II to state I.

As shown in Fig. 5, examine the parameters of the leg form in each phase of a cycle.

$$\varphi_1 = \theta_1 + \frac{\pi}{6} = 0.2861\pi \quad (5)$$

$$\theta_2 = arccos\frac{R'^2 + e^2 - R^2}{2R'e} = 0.1180\pi \quad (6)$$

$$d = \sqrt{R'^2 + e^2 - 2R'ecos\left(\theta_2 + \frac{2\pi}{3}\right)} = 120.6mm \quad (7)$$

$$\varphi_2 = arccos\frac{R'^2 + d^2 - e^2}{2R'd} + arcsin\frac{R}{d} = 0.2042\pi \quad (8)$$

$$\beta = arccos\frac{R - \sqrt{3}R'sin\left(\varphi_2 - \frac{\pi}{6}\right)}{R} = 0.2750\pi \quad (9)$$

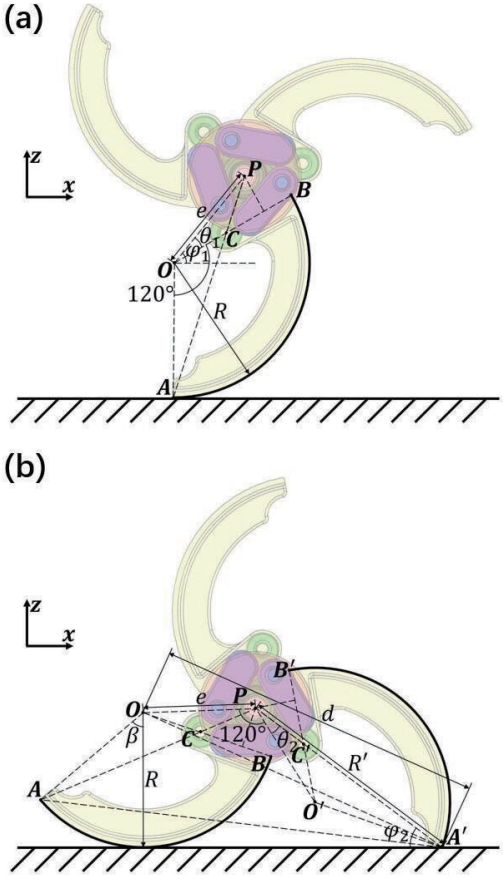

Fig. 5. Movement of the leg form on smooth roads. (a) State I. (b) State II.

The displacement of the overall center of mass of the mobile robot in the x, z-direction is represented by the displacement of the wheel center P in the x, z-direction, and the equation of the displacement of the wheel center P in the x, z-direction, using the horizontal ground as the z = 0 plane, are as follows:

$kT \le t < kT + t_1$:

$$x_P = ks + R\omega(t - kT) + ecos[\varphi_1 - \omega(t - kT)] - ecos\varphi_1 \quad (10)$$

$$z_P = R + esin[\varphi_1 - \omega(t - kT)] \quad (11)$$

$kT + t_1 \le t < (k+1)T$:

$$x_P = ks + s_1 + R'cos\varphi_2 - R'cos[\varphi_2 + \omega(t - t_1 - kT)] \quad (12)$$

$$z_P = R'sin[\varphi_2 + \omega(t - t_1 - kT)] \quad (13)$$

Derivation of the displacement equation of the wheel center P in the x, z-direction for time t respectively yields the velocity equation of the wheel center P in the x, z-direction respectively as:

$kT \le t < kT + t_1$:

$$v_x = R\omega + e\omega sin[\varphi_1 - \omega(t - kT)] \quad (14)$$

$$v_z = -e\omega cos[\varphi_1 - \omega(t - kT)] \quad (15)$$

$kT + t_1 \le t < (k+1)T$:

$$v_x = R'\omega sin[\varphi_2 + \omega(t - t_1 - kT)] \quad (16)$$

$$v_z = R'\omega cos[\varphi_2 + \omega(t - t_1 - kT)] \quad (17)$$

Where T is a period, t_1 is the duration of stage one in a period, s is the displacement of wheel center P in the x-direction in a period, s_1 is the displacement of stage one center P in the x-direction in a period, and k is the number of periods experienced before this period. The expressions of T, t_1, s, and s_1 are as follows:

$$T = \frac{2\pi}{3\omega} \quad (18)$$

$$t_1 = \frac{\beta}{\omega} \quad (19)$$

$$s = R\beta + R'cos\varphi_2 - R'cos\left[\varphi_2 + \omega\left(\frac{2\pi}{3\omega} - \frac{\beta}{\omega}\right)\right] \quad (20)$$

$$s_1 = R\beta \quad (21)$$

When the mobile robot moves along the positive direction of x-axis in leg-like form, we take the motor output speed ω = πrad/s and substitute the relevant data above to derive the displacement model and velocity model of the wheel center P in the x, z directions, as shown in Fig. 6.

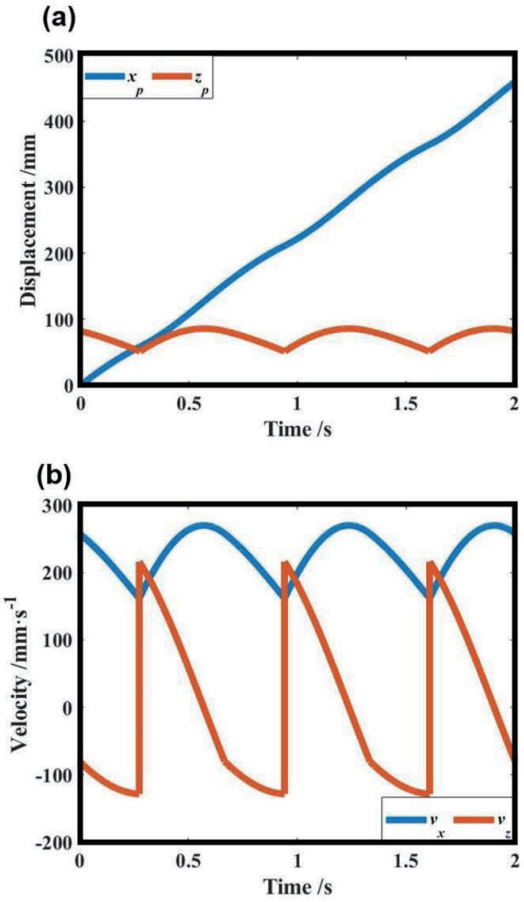

Fig. 6. Displacement model and velocity model of wheel center P in x, z-direction. (a) Displacement vs time. (b) velocity vs time.

2) Stable process of climbing obstacles in the leg form

Assuming that the mobile robot moves in the positive direction along the x-axis in the leg-like form to cross the barrier without slipping in the y-axis direction, each parameter of the whole moving process can be represented in the x-z plane. The two wheels located on one side of the vehicle body are selected for the study below.

As shown in Fig. 7, the front wheel rotates around the contact point A between one of its wheel feet and the top surface of the obstacle, thus driving the whole body over the obstacle. At this time, it is necessary to ensure that the front wheels are subjected to a large enough value of the support reaction force F_N and static friction force f at contact point A to make an effective contact between the front wheels and the top surface of the obstacle without slippage. Therefore, the values of the support reaction force F_N and the static friction force f in the process of crossing the obstacle should be analyzed.

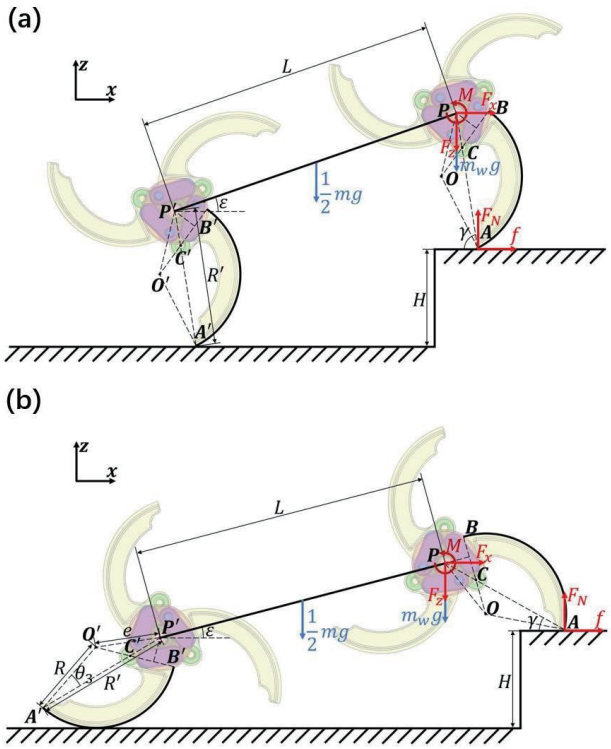

Fig. 7. Movement of leg form in obstacle clearance. (a) Progress I. (b) Progress II.

When the rigid body does uniform rotation, the vector sum of all external forces is directed by the center of mass to the axis of rotation, and the algebraic sum of moments for the axis of rotation is zero. Let the angular velocity of the uniform rotation of the wheel be ω. From this, the equilibrium equations of forces and moments can be listed for a front wheel:

$$F_x + f = m_w\omega^2 R' cos\gamma \tag{22}$$

$$F_z + m_w g - F_N = m_w\omega^2 R' sin\gamma \tag{23}$$

$$\tau + F_x R' sin\gamma = F_z R' cos\gamma + m_w g R' cos\gamma + M \tag{24}$$

Where F_x is the fraction of the force of the body on the front wheel in the horizontal direction; F_z is the fraction of the force of the body on the front wheel in the vertical direction; τ is the driving moment provided by the motor; and M is the equivalent moment of the body on the front wheel:

$$M = \frac{1}{4} mgLcos\varepsilon \tag{25}$$

It should be noted that the value of angle ε changes in the two processes. When the rear wheel rolls along the edge of the wheel $\widehat{AB}$ (Process I), the value of angle ε keeps getting larger; when the rear wheel rotates with the contact point A as the center (Process II), the value of angle ε remains constant. The expressions of angle ε for the two processes are obtained as follows:

Process I:

$$\varepsilon = arccos \frac{\sqrt{L^2 - \begin{bmatrix} H + R'sin\gamma - R'sin\left(\frac{\pi}{3} - \gamma\right) \\ -R + Rsin\left(\frac{\pi}{3} - \gamma + \theta_3\right) \end{bmatrix}^2}}{L} \tag{26}$$

Process II:

$$\varepsilon = arccos \frac{\sqrt{L^2 - H^2}}{L} = 0.1082\pi \tag{27}$$

Where:

$$\theta_3 = arccos \frac{R^2 + R'^2 - e^2}{2RR'} = 0.09589\pi \tag{28}$$

With the worst-case assumption, i.e., when the front wheel and the top surface of the obstacle are in a state where they will slip but not slide, satisfying:

$$f = \mu F_N \tag{29}$$

The expression of the support reaction force F_N at the contact point A of the front wheel in the two processes of crossing the barrier is obtained by associating with the above-balanced equations of forces and moments.

$$F_N = \frac{\tau - \frac{1}{4} mgLcos\varepsilon}{R'(cos\gamma + \mu sin\gamma)} \tag{30}$$

$$\tau = \frac{955P\pi}{3\omega} \tag{31}$$

The rated power of the motor P = 4.156×10^{-3}kW, from which the relationship between the support reaction force F_N and the angle γ and wheel speed ω is shown in Fig. 8.

As the rotational speed ω increases, the driving torque τ provided by the motor decreases, the branch reaction force F_N also decreases, and the wheeled-leg is likely to slip with the top surface of the obstacle, and the reliability of crossing the obstacle decreases; as the rotational speed ω decreases, the driving torque τ provided by the motor increases, and the ground reaction force F_N also increases, and the reliability of crossing the obstacle increases.

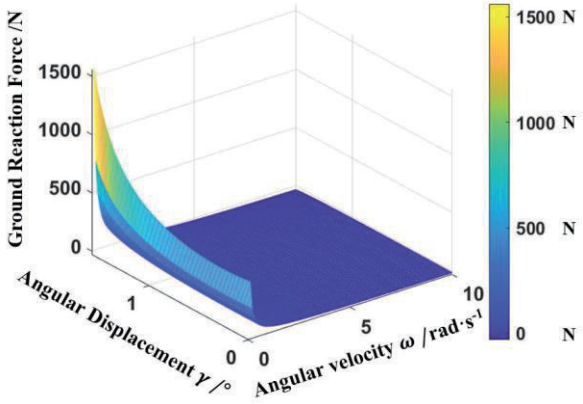

Fig. 8. Simulation result of Ground Reaction force in normal direction at contact point.

D. Optimize Deformation Control Strategy Based on Electromagnetic Clutch

After our research, the deformable wheel and leg mechanisms currently on the market can meet the basic motion requirements of robots by changing their forms, but most of them have greater difficulties in the process of deformation and leg state motion maintenance, so the deformable wheel and leg mechanism in the motion state deformation and form maintenance methods are particularly important.

Herein, we propose a high-frequency pulse-based electromagnetic clutch control strategy. In a given period T, the duty cycle is set to ξ. In $T\xi$ time, the output is high level, the electromagnetic clutch is energized and does not restrict the rotation of the deformable axle, and the deformable axle rotates with the power input axis due to the friction between the parts, the friction between the wheel and the ground and the gravity, and there is no relative motion between the two; in $T(1-\xi)$ time, the output is low level, the electromagnetic clutch the relative motion is generated between the deformation axis and the power input axis, and the driving force is transmitted to the end of the wheel through the four-bar mechanism to offset the reaction force from the horizontal ground to the end of the wheel, to achieve the purpose of preventing the natural transition from the leg state which is not easy to maintain to the wheel state which is easy to maintain. Of course, this natural transition is what we do not want to see.

Frequent power on and off in a short period (<1s), to achieve the effect of "damping" and maintain the stability of the motion in the leg state. The damping factor c is a function of duty cycle ξ and frequency f.

$$c = g(\xi, f) \tag{32}$$

According to Newton's second law, the input dynamics can be expressed by the angular velocity $\dot{\theta}$ and the angular acceleration $\ddot{\theta}$.

$$N(t) = c\dot{\theta} + m\ddot{\theta} \tag{33}$$

The transfer function of this second-order system is thus easily obtained as follows.

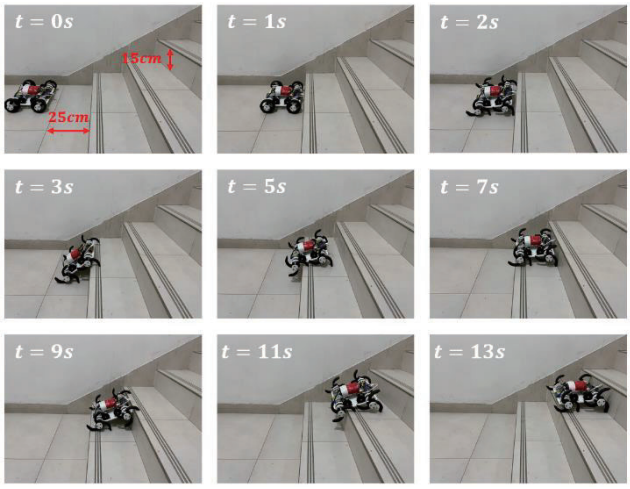

$$G(s) = \frac{\theta(s)}{N(s)} = \frac{1}{ms^2 + cs} = \frac{1}{s} \cdot \frac{1}{ms + c} \tag{34}$$

This is a typical type I system in automatic control theory, which is non-differential to the unit step input and has strong robustness.

III. Experimental Results

After technical feasibility and locomotion capability evaluation, the QuWheeleg robot was designed and built, as shown in Fig. 9. A fully assembled robot consists of four transformable wheels and the main body chassis. The chassis and deformation shaft are 3D printed with photosensitive resin material, and the main stress parts such as leg segment and power rod are also 3D printed with nylon.

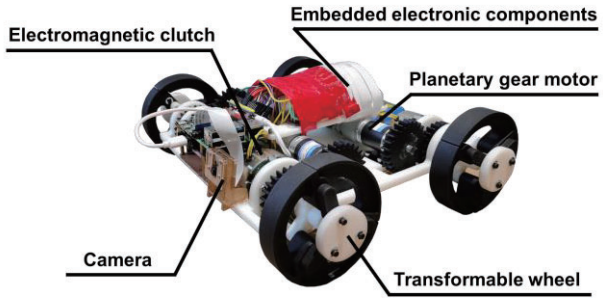

Fig. 9. The overall structure of QuWheeleg.

Since the obstacle climbing experiment can reflect the whole process of robot obstacle-negotiation process, this paper uses this experiment to analyze the obstacle-climbing capability of QuWheeleg robot.

The parameters of this experiment are: (1) the height of the step is 150mm; (2) the angular speed of the motor drive is 0.8rad/s.

Fig. 10. Sequence diagram of obstacle crossing experiment.

The whole moving process can be divided into four stages.

(1) t = 0~2s, wheel-leg switching. The robot approaches the step in a wheeled state, touches the step at t = 1s, changes from a wheeled state to a leg state by remote control, and completes the change at t = 2s.

(2) t = 2~5s, the first overturning. The robot climbs the first step in the leg state, and the overrunning leg rides on the first step at t = 3s. The contact point between the overrunning leg and the first step is the center of rotation, and the robot's center of gravity is driven upward by the rotation of the motor.

(3) t = 5~7s, self-adjustment. Observation of the robot's state at t = 5s shows that the robot is far from the second step, so the overrunning leg can't reach the second step within the next 2π/3 angle of the motor rotation. The robot can reach the height of the second step by crossing the barrier leg.

(4) t = 7~13s, the second overturning. The robot climbs up the second step in a leg-like state, and the overrunning leg rides on the second step at t = 9s. The contact point between the overrunning leg and the second step is the center of rotation, and the robot's center of gravity is driven upward by the rotation of the motor. Up to this point, the robot has completed the continuous overturning of the two steps.

The robot was first transformed from a wheel to a leg and then crossed the step smoothly. The experimental process shows that the deformed wheeled-leg mobile robot has the expected deformation and obstacle-crossing capability. The experimental results are consistent with the results of the kinematic analysis above, which also meet our expectations.

In addition, we noticed that the angular speed of the motor rotation and the pulse period of the electromagnetic clutch have a very important effect on the robot's overrun performance. For this reason, we conducted three experiments to investigate the effects of wheel speed ω and pulse period T on the robot's performance.

The test results of obstacle-climbing success rate are shown in TABLE II& III. To achieve good obstacle-negotiation stability and success rate, the rotating speed ω of the actuator and the pulse period T of the electromagnetic clutch should both be small. This is consistent with the previous theoretic analysis mentioned above.

The first experiment does not use the high-frequency pulse-based electromagnetic clutch control method, in the motor speed ω for a certain value of the conditions, let the robot try to go over a certain height of the steps, so-called a group of experiments. Each group of experiments is conducted three times, with green representing all three times are successed, yellow representing twice, orange representing once, and red representing all failures. The results of the experiments are shown in TABLE II. Observation of the experimental results shows that as the motor speed ω increases, the robot's overrun performance decreases, which is consistent with the results of

the kinematic analysis in Section II; and as the overrun height increases, the robot's overrun performance decreases, which is also consistent with the natural law.

TABLE II. STATISTICS ANALYSIS OF OBSTACLE-CLIMBING SUCCESS RATE WITHOUT PULSE CONTROL

ω(rad/s)	Obstacle height(mm)					
	50	70	90	110	130	150
0.4						
0.8			>50%			
1.2						
1.6				<50%		
2	0%					
2.4						

In the second experiment, the electromagnetic clutch control method based on high-frequency pulses was adopted, and the pulse period T = 2s was set to a certain value of the motor speed ω, and the robot was allowed to try to go over a certain height of the step, and the results of the first two experiments were compared.

TABLE III. STATISTICS ANALYSIS OF OBSTACLE-CLIMBING SUCCESS RATE UNDER PULSE CONTROL

ω(rad/s)	Obstacle height(mm)						T(s)
	50	70	90	110	130	150	
0.4							
0.8							
1.2			100%			>50%	2
1.6							
2						0%	
2.4			>50%				
1.2							0.5
							1
			100%				1.5
						>50%	2
					0%		2.5

Finally, we keep the motor speed ω fixed (ω = 1.2 rad/s) and take the pulse period T as the independent variable, and observe the results of the third experiment to find that the robot's overrun performance decreases as the pulse period T increases, which is consistent with the analysis results in Section II. Comparing the results of the three experiments (the pulse period T of the first experiment is regarded as infinity), it can be confirmed that the electromagnetic clutch control method based on high-frequency pulses is effective in improving the robot's overrun performance, and the robot's overrun performance increases as the pulse period T shortens. However, the same experimental results for pulse period T = 0.5~1.5s (good overrun performance for all heights) also warn us that it is meaningless to increase the pulse frequency, and it is good to keep the pulse period around 1s; similarly, the robot's overrun performance is similar when the motor speed ω = 0.4~0.8rad/s, and then we need to take into account the mobility performance The motor speed ω = 0.4~0.8 rad/s, the robot's performance is similar to that of the robot. Accordingly, it can be noted that the stability of maintaining the leg-like motion state decreases as the pulse period T is prolonged and the duty cycle ξ is increased.

IV. CONCLUSION AND FUTURE WORK

In this paper, an active deformation wheel mechanism based on a planar four-bar mechanism and an electromagnetic clutch high-frequency pulse control method is proposed for the prototype design of a mobile robot chassis for search and rescue tasks. Based on the design, analysis, and experiments of the prototype, the following conclusions can be drawn.

(1) The active deformation wheel mechanism design method is based on a planar four-bar mechanism, based on a genetic algorithm to optimize the deformation ratio, the optimized deformation ratio is 1.72, which ensures a strong performance in overcoming obstacles.

(2) Propose an active motion mode switching mechanism based on an electromagnetic clutch, which ensures the stability and reliability of robot mode switching without adding extra drive. The high-frequency pulse control method of the electromagnetic clutch is proposed, which significantly enhances the continuity of the leg mode motion state.

(3) Through simulation and experimental verification, the robot motion performance and stability test and the overrun performance experiment were completed. The experiments demonstrate the good over-block performance (150% body length) and efficient and stable motion as well as high load capacity (2kg) of the robot, which combines the advantages of wheel and leg motion and provides a reference for the design of other mobile robots, which can be applied in the fields of search and rescue and aerospace exploration in complex land environments after disasters.

ACKNOWLEDGMENT

This work was supported by the National Natural Science Foundation of China under Grant 62022014.

REFERENCES

[1] T. Thomas and S. Roland, “Mobility evaluation of wheeled all-terrain robots,” Robotics and Autonomous Systems, vol. 58, no. 5, pp. 508-519, 2010.

[2] Q. Shi et al., "Development of a Small-Sized Quadruped Robotic Rat Capable of Multimodal Motions," in IEEE Transactions on Robotics, doi: 10.1109/TRO.2022.3159188.

[3] A. Velimirovic, M. Velimirovic, and Institute of Electric and Electronic Engineer, “A new architecture of robot with ‘wheels-with-legs’(WWL),” in Advanced Motion Control, 1998, pp. 434-439.

[4] Y. Sugiyama and S. Hirai, “Crawling and jumping by a deformable robot,” International Journal of Robotics Research, vol. 25, no. 5/6, pp. 603-620, 2006.

[5] O. Siddharth, P. Stephen Prior, K. Mehmet, and S. Siu-Tsen, “Increasing the Trafficability of Unmanned Ground Vehicles through Intelligent Morphing,” in 2009 International Conference on Reconfigurable Mechanisms and Robots, 2009, pp. 674-681.

[6] C. Zheng and K. Lee, “WheeLeR: Wheel-Leg Reconfigurable Mechanism with Passive Gears for Mobile Robot Applications,” in 2019 International Conference on Robotics and Automation (ICRA), 2019, pp. 9292-9298.

[7] Y. S. Kim, G. P. Jung, H. Kim, K. J. Cho, and C. N. Chu, “Wheel Transformer: A Wheel-Leg Hybrid Robot With Passive Transformable

Wheels," IEEE Transactions on Robotics: A publication of the IEEE Robotics and Automation Society, vol. 30, no. 6, pp. 1487-1498, 2014.

[8] D. Y. Lee, G. P. Jung, M. K. Sin, and S. H. Ahn, "Deformable wheel robot based on origami structure," in IEEE International Conference on Robotics and Automation, 2013, pp. 5612-5617.

[9] Q. Shi et al., "Implementing Rat-Like Motion for a Small-Sized Biomimetic Robot Based on Extraction of Key Movement Joints," in IEEE Transactions on Robotics, vol. 37, no. 3, pp. 747-762, June 2021, doi: 10.1109/TRO.2020.3033705.

[10] Hen-Wei Huang, Jack Chen, Peter R. Chai, Claas Ehmke, Philipp Rupp, Farah Z. Dadabhoy, Annie Feng, Canchen Li, Akhil J. Thomas, Marco da Silva, Edward W. Boyer, Giovanni Traverso, "Mobile Robotic Platform for Contactless Vital Sign Monitoring", Cyborg and Bionic Systems, vol. 2022, Article ID 9780497, 11 pages, 2022.

[11] Lei Wang, Libo Meng, Ru Kang, Botao Liu, Sai Gu, Zhihao Zhang, Fei Meng, Aiguo Ming, "Design and Dynamic Locomotion Control of Quadruped Robot with Perception-Less Terrain Adaptation", Cyborg and Bionic Systems, vol. 2022, Article ID 9816495, 10 pages, 2022.

[12] Luyao Wang, Lihua Ma, Jiajia Yang, Jinglong Wu, "Human Somatosensory Processing and Artificial Somatosensation", Cyborg and Bionic Systems, vol. 2021, Article ID 9843259, 11 pages, 2021.

[13] X. Wang, X. Xu, Z. Feng and H. Wu, "Structural Optimization Design and Performance Simulation of A Novel Six-wheel-legged Mobile Robot," 2018 IEEE International Conference on Robotics and Biomimetics (ROBIO), 2018, pp. 206-1352, doi: 10.1109/ROBIO.2018.8665104.

[14] J. Liu and J. Yang, "Design and mode switching of wheel-leg adaptable amphibious robot," 2017 2nd Asia-Pacific Conference on Intelligent Robot Systems (ACIRS), 2017, pp. 270-274, doi: 10.1109/ACIRS.2017.7986106.

[15] M. R. Vazifeh Ardalani, A. Toorani and A. H. Korayem, "Design and construction of a wheel-leg robot and testing the robot for different motion scenarios," 2022 8th International Conference on Control, Instrumentation and Automation (ICCIA), 2022, pp. 1-6, doi: 10.1109/ICCIA54998.2022.9737205.

[16] Y. Xiang et al., "Powered Super Tail: A Terrain-Adaptive Wheel-legged Robotic Limb to Assist Human's Load Carriage," 2021 27th International Conference on Mechatronics and Machine Vision in Practice (M2VIP), 2021, pp. 676-681, doi: 10.1109/M2VIP49856.2021.9665086.

[17] S. Cheong et al., "Supervised Autonomy for Remote Teleoperation of Hybrid Wheel-Legged Mobile Manipulator Robots," 2021 IEEE/RSJ International Conference on Intelligent Robots and Systems (IROS), 2021, pp. 3234-3241, doi: 10.1109/IROS51168.2021.9635997.

[18] H. Zhou, H. Yu, X. Li, H. Feng, S. Zhang and Y. Fu, "Configuration Transformation of the Wheel-Legged Robot Using Inverse Dynamics Control," 2021 IEEE International Conference on Robotics and Automation (ICRA), 2021, pp. 3091-3096, doi: 10.1109/ICRA48506.2021.9560781.

[19] K. Xu, S. Wang, X. Wang, J. Wang, Z. Chen and D. Liu, "High-Flexibility Locomotion and Whole-Torso Control for a Wheel-Legged Robot on Challenging Terrain," 2020 IEEE International Conference on Robotics and Automation (ICRA), 2020, pp. 10372-10377, doi: 10.1109/ICRA40945.2020.9197526.

[20] V. S. Medeiros, E. Jelavic, M. Bjelonic, R. Siegwart, M. A. Meggiolaro and M. Hutter, "Trajectory Optimization for Wheeled-Legged Quadrupedal Robots Driving in Challenging Terrain," in IEEE Robotics and Automation Letters, vol. 5, no. 3, pp. 4172-4179, July 2020, doi: 10.1109/LRA.2020.2990720.